Application of Micro-Tubing Reeling System to Serial Femtosecond Crystallography

Jihan Kim , Sehan Park , Yunje Cho , Jaehyun Park *

Posted Date: 20 December 2023

doi: 10.20944/preprints202312.1545.v1

Keywords: SFX; reeling; sample delivery; lysozyme; PAL-XFEL

Article

Application of Micro-Tubing Reeling System to Serial Femtosecond Crystallography

Jihan Kim [1,#], Sehan Park [2,#], Yunje Cho [1] and Jaehyun Park [2,*]

[1] Department of Life Sciences, Pohang University of Science and Technology, Pohang 37673, Republic of Korea

[2] Pohang Accelerator Laboratory, Pohang University of Science and Technology, Pohang 37673, Republic of Korea

* Correspondence: jaehyun.park@postech.ac.kr

[#] Equally contributed to this work.

Abstract: Microcrystal delivery instruments are pivotal to perform serial femtosecond crystallography experiments at the XFEL facilities. We present a novel sample delivery technique based on a micro-tubing reeling system (MRS). Even though the tiny size of the micro-tubing, the MRS device has an advantage of operation without real-time position adjustment of the tube to match with the XFEL pulses. Moreover, the applicable repetition rate is more flexible than the previously reported chip-based one-dimensional fixed target system.

Keywords: SFX; reeling; sample delivery; lysozyme; PAL-XFEL

1. Introduction

X-ray Free Electron Laser (XFEL) sources have enabled to reveal various macromolecular structures based on the "diffraction before destruction" scheme [1]. The three-dimensional electron density map can be obtained at room temperature with quite low radiation damage effect through serial femtosecond crystallography (SFX) [2–5]. To perform SFX, micron sized crystals should be placed at the XFEL interaction point continuously.

For this purpose, various attempts have been made to develop sample delivery techniques such as liquid jet with a gas dynamic virtual nozzle [6,7], lipidic cubic phase (LCP) injection [8], fixed sample scanning [9–11], sandwiched thin films [12–14], and concentric MESH [15].

The key requirements for the sample delivery are sample consumption, stable transport, and prevention from dehydration during the SFX experiments. Liquid jet and LCP injections are advantageous for lower background scattering and slow sample delivery speed, respectively. However, they have drawbacks with the high sample consumption and high background scattering from the viscous media for each. Approach to use thin films has a merit on the simpler sample preparation and delivery but still requires additional efforts to achieve viscous environments or the attachment of two thin films to prevent sample dehydration. On the other hand, the one-dimensional fixed target utilizing micro-tubing takes strong points of previous techniques like low background scattering intensity, controllable delivery speed related to sample consumption, and quick closing process for keeping almost a perfect hydration condition.

In the previous research, we have reported a chip-based one-dimensional fixed target system which consists of a two-dimensional array of the microcrystal containers (MCCs) [16]. A single chip holds four MCCs and the ID, OD, and length of the MCC are 100 μm, 126 μm, and 500 mm, respectively. The sample, usually solution of protein microcrystals, is inserted into the MCC and XFEL pulses are illuminated on the tubing with the raster scanning method. The MCC facilitates less sample consumption than the two-dimensional fixed target and a long-lasting humid condition. From the instrument point of view, due to the micron-sized tube diameter, the illumination on the tube by the XFEL pulses can be missed even for a tiny angular misalignment during a scan. To clear this alignment issue, we have embedded a position feedback control via a real-time visual servo

Preprints (www.preprints.org) | NOT PEER-REVIEWED | Posted: 20 December 2023 doi:10.20944/preprints202312.1545.v1

method. However, this operational scheme has a limitation on the applicable XFEL repetition rate owing to the time lag originated from real-time image processing to identify positions of the MCC and immediate movement of the MCC to the aimed XFEL position. Here, we report a novel micro-tubing-based sample delivery system, called micro-tubing reeling system, with advanced features of simplified XFEL beam alignment process, without the real-time position feedback, and expanding feasible XFEL repetition rate to apply for SFX experiments.

2. Micro-tubing reeling system

The micro-tubing reeling system (MRS) is a novel instrument to deliver microcrystals to the X-ray interaction point for serial crystallography experiments at the synchrotron and XFEL facilities. Figure 1a shows the drawing of the MRS system and components. Different from the previous operation scheme based on the fixed frame, the position of the MCC, which is a micro-tubing container holding microcrystals inside, is controlled through winding it to a reel. It is designed to have the MCC, single mini-rotor, two tube guides and a tensioner tube. The mini-rotor is a 2-phase stepping motor (Microservo Encoding-motor PGM22-2028E). The first preparation step before the sample loading on the MCC is stringing three pieces of PEEK tube (Part No. 1531, IDEX health and science) on the polyimide micro-tubing (length: 1000 mm, inner diameter: 100 μm, thickness: 13 μm, Nordson Corp.) working as the MCC. The inner and outer diameter of the PEEK tubes are 0.01 and 1/16 in, respectively. The length of two short PEEK tubes pieces is about 15 mm and the other piece is about 45 mm. Here, the two short and a longer PEEK tubing pieces are played as the MCC traveling guide and tensioner (Figure 1b). These two short PEEK tubing is placed on a groove and settled with the cover plate installed by the four magnets.

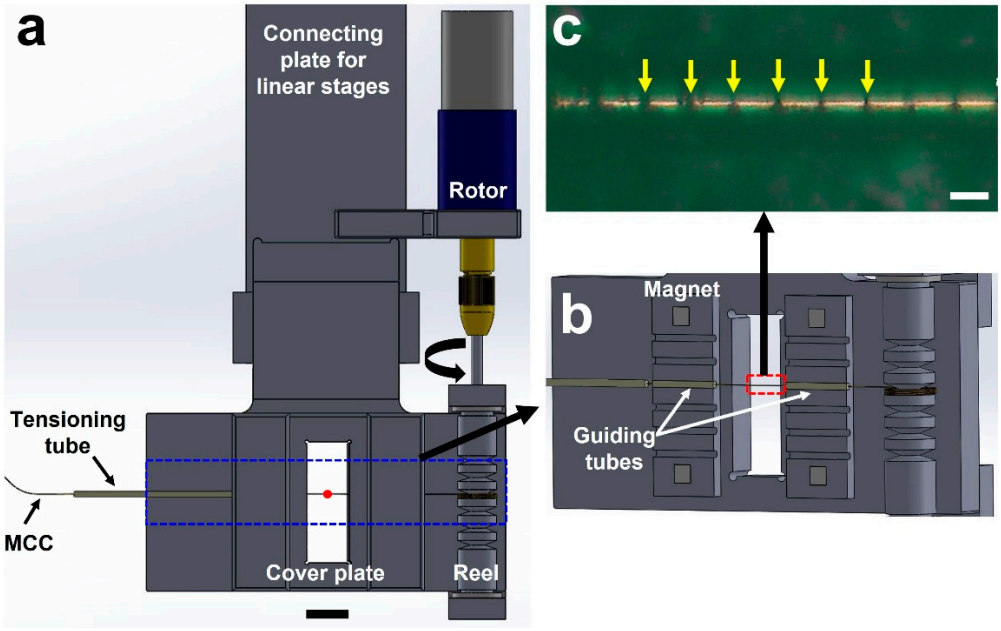

Figure 1. (a) Geometry of micro-tubing reeling system (b) Guiding tubes to maintain trajectory of the MCC (c) Holes generated by XFEL pulses on the MCC (white bar = 50 μm).

A sample such as microcrystals suspended solution is inserted into the MCC. A commercial fast-drying glue (LOCTITE® 401) is used to close both sides of the MCC. This MCC-based sample delivery technique can control the delivery speed matching XFEL repetition rate and does not cause a clogging which can be encountered when using liquid jet or LCP injectors.

Generally, the tension control is tricky to make a stable delivery like a conveyer belt. Most of the tension control system is not straightforward. Several kinematic designs are usually employed to make a proper tension level. Damping wheel, compensation body, and dancing lever schemes are

 doi:10.20944/preprints202312.1545.v1

mostly used to maintain the tension level. They require various pullies and translational stages to keep the continuous reeling motion [17].

On the other hand, the MRS has a simpler tensioner structure than prototypical schemes that controlled by the pullies and translational stages. The tension is offered by an interaction between the MCC and a tensioner tube which is a short piece of PEEK tubing that has length, inner and outer diameter of about 40 mm, 0.01" and 1/16", respectively. The tension comes from the resistance of the MCC motion with curvature of PEEK tubing. The radius of the curvature was about 160 mm. Under this geometry, the delivery motion is very stable during the data collection (Supplementary movie 1).

Sample loading on the MCC is exactly same with the methods that described in the previous study [16]. The needle of the syringe that containing crystal mixed solution is connected with the MCC by a union fitting. The both ends of the MCC is closed with a fast-drying glue to maintain humidity during handling and experiments. To install the prepared MCC on the MRS system, one end of the MCC is attached to the reeling parts with adhesive tapes and closed with the cover frame. The cover frame of the reel also has a magnetic mount for a quick installation.

3. Experiments and Results

3.1. Experimental condition and data acquisition

We have performed the SFX experiments to verify the application of the MRS sample delivery at the NCI experimental station, PAL-XFEL [18–20]. The wavelength, pulse duration, and photon flux for the incident XFEL were 1.0 Å, < ~ 25 fs, and ~ 2 x 10^{11} photons per pulse, respectively. The bandwidth of XFEL is approximately 0.2 %. The focused beam size delivered by the Kirkpatrick–Baez mirrors was approximately 5 x 5 μm^2 at the sample position [21]. The diffraction images were collected with MX225-HS detector (Rayonix, LLC, Evanston, IL, USA) at the distance of about 150 mm from the sample position. The 4 x 4 binning mode was utilized for the detector to match the incident XFEL repetition rate of 30 Hz. The Hen egg white (HEW) lysozyme micro crystals have been used as a model sample without additional carrier matrix media. The crystal size was about 5 x 5 x 5 μm^3. The sample consumption for the whole data collection was about 50μl.

3.2. Operation of the MRS

The MRS is installed and can be operated in the MICOSS, a SFX dedicated sample chamber established to operate various type of injectors at the PAL-XFEL [22]. Figure 2 shows the photos of the MRS and installed geometry inside of the MICOSS. The position of the MRS is manipulated with 3-axis linear stages [22]. The mini-rotor of the MRS is remotely controlled through a feedthrough which makes a connection between the 2-phase stepping motor and customized controller. The angle of the motor is manipulated with the number of square pulses. The number of pulses to make a single turn is 2868. The tangential speed of the tubing is about 1.8 mm/sec to have a 60 μm spacing between the consecutive illumination by the incoming XFEL pulses as showin on the Figure 1c. The effective length of the tubing is about 950 mm except for the rest portion which has been used for attaching the MCC to the mini-rotor. Then the operation time is about 9 min per a single tubing, which is matched with a data acquisition time. We have used three MCCs to collect diffraction images.

Preprints (www.preprints.org) | NOT PEER-REVIEWED | Posted: 20 December 2023 doi:10.20944/preprints202312.1545.v1

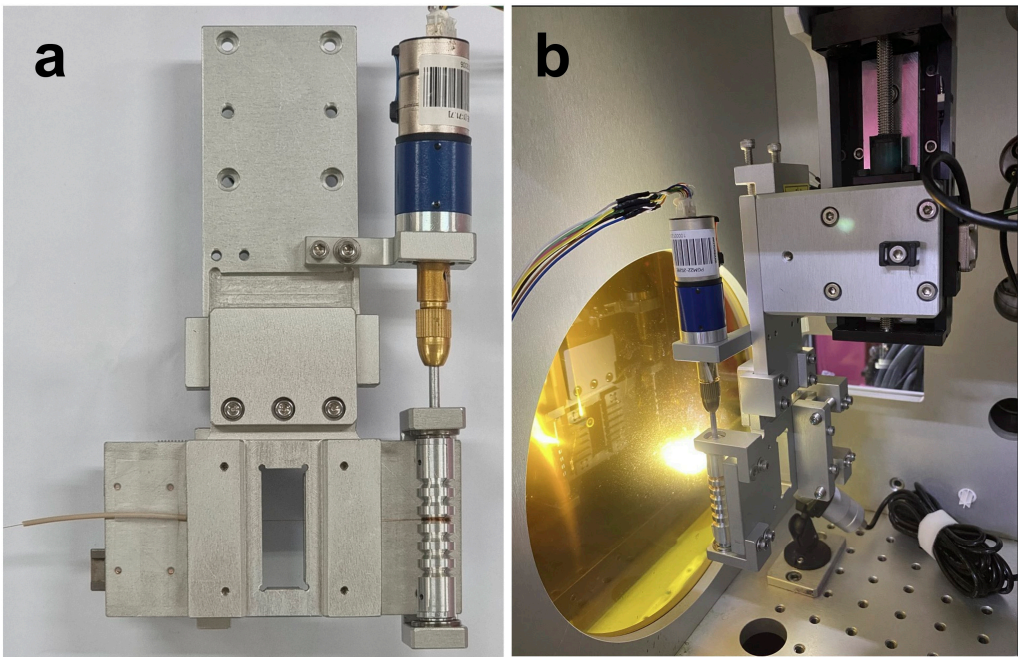

Figure 2. (a) Photo of the MRS unit (b) Installation image of the MRS unit in the MICOSS at the NCI endstation of the PAL-XFEL.

3.3. Structure analysis of lysozyme

We have used the lysozyme micro crystals without an additional carrier matrix media to determine room-temperature structure by the SFX experiment. The total number of collected images is 44,272 and the hitting ratio was about 49 %. In addition, the frames of 42.2% out of the classified images were indexed, integrated, and merged in point group 4/mmm to a resolution cutoff of 1.8 Å with the CrystFEL suite [23–26]. Figures of merit were calculated using compare_hkl (R_{split}, $CC_{1/2}$, and CC*) and check_hkl (SNR, multiplicity, and completeness) softwares. The phase has been retrieved by the molecular replacement method with the Phenix [27], utilizing the lysozyme structure which was previously deposited in the PDB (ID: 4ET8). Model building and structure refinement were performed with the coot [28]. The data collection and refinement statistics are given in Table 1. The electron density map of lysozyme was very clear throughout the amino acid sequence from Lys19 to Leu147 (Figure 3). The lysozyme structure determined by MRS showed high similarity with a previously deposited lysozyme structure (PDB ID: 4ET8) [2] with R. M. S. Deviaton of 0.121 Å for all C-α atoms. The electron density map shows some additional density for water molecules. In the refined lysozyme structure, no signs of the radiation damage were observed.

Preprints (www.preprints.org) | NOT PEER-REVIEWED | Posted: 20 December 2023 doi:10.20944/preprints202312.1545.v1

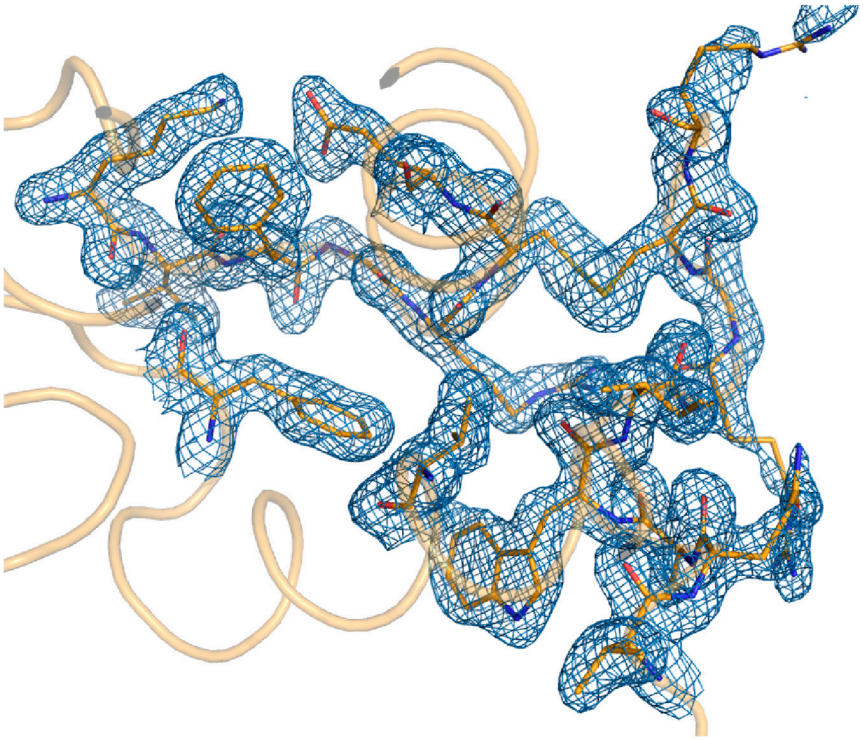

Figure 3. 2Fo-Fc electron density map of lysozyme defined by the MRS at 293K. 2Fo-Fc electron density map (blue mesh, 1σ) is shown with the surface region of Hen egg white lysozyme (orange).

Table 1. Data collection and refinement statistics. [a] The values in parentheses are for highest-resolution shell. [b] $R_{split} = \left(1/\sqrt{2}\right) \cdot \frac{\Sigma_{hkl}|I_{hkl}^{even} - I_{hkl}^{odd}|}{\frac{1}{2}|I_{hkl}^{even} - I_{hkl}^{odd}|}$. [c] The free set represents a random 5% of reflections not included in refinement.

Data collection	Lysozyme
PDB code	8JQV
Wavelength (Å)	Å
Exposure time	50 fs
Space group	P $4_3 2_1 1$
Cell dimensions	
a,b,c (Å)	79.3, 79.3, 38.3
α, β, γ (°)	90.0, 90.0, 90.0
No. of Collected image	44272
No. of Hit image	21633
No. of Indexed image	9132
Resolution (Å)	50-1.80(1.87-1.80)[a]
No. of Unique reflections	12462(1224)
Completeness (%)	100(100)
Redundancy	335.6(233.8)
SNR	3.62(1.36)
R_{split}[b]	25.98(78.87)
CC	0.91(0.42)
CC*	0.98(0.77)
Wilson B-factor (Å^2)	32.17
Refinement statistics	
Resolution (Å)	39.65-1.80 (1.94-1.80)
R-work	0.2040 (0.3772)

 doi:10.20944/preprints202312.1545.v1

R-free[c]	0.2302 (0.3911)
R.m.s. deviations	
Bond (Å)	0.006
Angle (°)	0.879
Average B-factor(Å^2)	
Protein	29.07
Water	35.78
Clash score	3.06
Ramachandran (%)	
Favored	97.64
Allowed	2.36
Rotamer outlier (%)	0.00

4. Discussion and conclusion

A novel microcrystal delivery technique has been developed by employing mini-rotor which winds the MCC according to the designated speed. Different from the previous setup serving real-time position feedback with visual servo scheme, it doesn't require image processing during the scanning. It means that the applicable XFEL repetition rate can be increased by simply adjusting the rotational speed since there is no time lag for the image processing and position feedback.

For the stable operation, the MCC should travel at a flat trajectory. To accomplish and maintain this motion control, a proper tension and travel guides for the MCC should be adopted. In the aspect of size of the instrument, however, the compactness is one of the advantageous features regarding the instrumental handling and space constraints at the beamlines.

This simple structure of tensioner and guides of the MRS system provides an adequate tension for stable operation of the reeling system. The applied pressure on the MCC during the operation can be estimated as a criterion for the stable operation. The mini-rotor rotates a single turn with 2868 pulses provided from the motor controller. The time for a single turn of the mini-rotor is about 12.9 seconds. Then, it leads to the pulse rate of about 222 pps (pulses per second). Approximately, it corresponds to the torque value of about 70 gf ·cm (in cgs unit) or 0.36 mN·m (in mks unit) (Figure S1). Since the radius of the rotor for reeling is 3.7 mm, the tangential force applied on the MCC for the corresponding torque is estimated as 97 mN. Considering the inner diameter and thickness of the MCC, the cross-sectional area to the length direction is about 4.08 x 10^3 μm^2. Then the applied pressure on the MCC is calculated as about 23.8 MPa. This value is below of the Yield strength of polyimide material of 13 μm thick as 69 MPa [29]. It implies that the stable operation of the MRS works is feasible while making a flat traveling of the MCC. The stable operation of the MRS also can be observed from the movie taken with a long working distance microscope which monitors the sample delivery during the experiment (Video S1).

The demonstration through the SFX experiment concludes that the MRS has the opportunities to overcome previous issues on the previously developed 1D fixed target based on the chip design. The operation is quite stable without any real-time position feedback to match the XFEL beam illumination position on the MCC. Since the MRS can omit the position calculation time of the MCC along with the operation, the applicable repetition rate of XFEL source can be beyond the limited value given by the previous 1D fixed target [16].

Supplementary Materials: The following supporting information can be downloaded at the website of this paper posted on Preprints.org, Figure S1: The relation between the pps and torque; Video S1: Operation of the MRS observed by the long-working distance microscope installed at the beamline.

Author Contributions: Conceptualization, J.K. and J.P.; methodology, S.P., J.P.; formal analysis, J.K.; data curation, J.K., S.P. and J.P; writing—original draft preparation, J.K and J.P.; supervision, Y.C. and J.P.; funding acquisition, Y.C. and J.P. All authors have read and agreed to the published version of the manuscript.

Funding: This research was funded by National Research Foundation of Korea, grant No. NRF-2017M3A9F6029733 to JP.

Acknowledgments: The authors acknowledge the accelerator and beamline departments at the PAL-XFEL for the technical supports.

Conflicts of Interest: The authors declare no conflict of interest.

References

1. Neutze, R.; Wouts, R.; van der Spoel, D.; Weckert, E.; Hajdu, J. Potential for biomolecular imaging with femtosecond X-ray pulses. *Nature* **2000**, *406* (6797), 752-757.
2. Boutet, S.; Lomb, L.; Williams, G. J.; Barends, T. R.; Aquila, A.; Doak, R. B.; Weierstall, U.; DePonte, D. P.; Steinbrener, J.; Shoeman, R. L.; et al. High-resolution protein structure determination by serial femtosecond crystallography. *Science* **2012**, *337* (6092), 362-364.
3. Chapman, H. N.; Fromme, P.; Barty, A.; White, T. A.; Kirian, R. A.; Aquila, A.; Hunter, M. S.; Schulz, J.; DePonte, D. P.; Weierstall, U.; et al. Femtosecond X-ray protein nanocrystallography. *Nature* **2011**, *470* (7332), 73-77.
4. Liu, W.; Wacker, D.; Gati, C.; Han, G. W.; James, D.; Wang, D.; Nelson, G.; Weierstall, U.; Katritch, V.; Barty, A.; et al. Serial femtosecond crystallography of G protein-coupled receptors. *Science* **2013**, *342* (6165), 1521-1524.
5. Spence, J. C. H.; Weierstall, U.; Chapman, H. N. X-ray lasers for structural and dynamic biology. *Rep Prog Phys* **2012**, *75* (10).
6. DePonte, D. P.; Doak, R. B.; Hunter, M.; Liu, Z.; Weierstall, U.; Spence, J. C. SEM imaging of liquid jets. *Micron* **2009**, *40* (4), 507-509.
7. Deponte, D. P.; McKeown, J. T.; Weierstall, U.; Doak, R. B.; Spence, J. C. Towards ETEM serial crystallography: Electron diffraction from liquid jets. *Ultramicroscopy* **2011**, *111* (7), 824-827.
8. Weierstall, U.; James, D.; Wang, C.; White, T. A.; Wang, D.; Liu, W.; Spence, J. C.; Bruce Doak, R.; Nelson, G.; Fromme, P.; et al. Lipidic cubic phase injector facilitates membrane protein serial femtosecond crystallography. *Nat Commun* **2014**, *5*, 3309.
9. Oghbaey, S.; Sarracini, A.; Ginn, H. M.; Pare-Labrosse, O.; Kuo, A.; Marx, A.; Epp, S. W.; Sherrell, D. A.; Eger, B. T.; Zhong, Y.; et al. Fixed target combined with spectral mapping: approaching 100% hit rates for serial crystallography. *Acta Crystallogr D Struct Biol* **2016**, *72* (Pt 8), 944-955.
10. Roedig, P.; Ginn, H. M.; Pakendorf, T.; Sutton, G.; Harlos, K.; Walter, T. S.; Meyer, J.; Fischer, P.; Duman, R.; Vartiainen, I.; et al. High-speed fixed-target serial virus crystallography. *Nat Methods* **2017**, *14* (8), 805-810.
11. Sherrell, D. A.; Foster, A. J.; Hudson, L.; Nutter, B.; O'Hea, J.; Nelson, S.; Pare-Labrosse, O.; Oghbaey, S.; Miller, R. J.; Owen, R. L. A modular and compact portable mini-endstation for high-precision, high-speed fixed target serial crystallography at FEL and synchrotron sources. *J Synchrotron Radiat* **2015**, *22* (6), 1372-1378.
12. Doak, R. B.; Nass Kovacs, G.; Gorel, A.; Foucar, L.; Barends, T. R. M.; Grunbein, M. L.; Hilpert, M.; Kloos, M.; Roome, C. M.; Shoeman, R. L.; et al. Crystallography on a chip - without the chip: sheet-on-sheet sandwich. *Acta Crystallogr D Struct Biol* **2018**, *74* (Pt 10), 1000-1007.
13. Hunter, M. S.; Segelke, B.; Messerschmidt, M.; Williams, G. J.; Zatsepin, N. A.; Barty, A.; Benner, W. H.; Carlson, D. B.; Coleman, M.; Graf, A.; et al. Fixed-target protein serial microcrystallography with an x-ray free electron laser. *Sci Rep* **2014**, *4*, 6026.
14. Lee, D.; Baek, S.; Park, J.; Lee, K.; Kim, J.; Lee, S. J.; Chung, W. K.; Lee, J. L.; Cho, Y.; Nam, K. H. Nylon mesh-based sample holder for fixed-target serial femtosecond crystallography. *Sci Rep* **2019**, *9* (1), 6971.
15. Sierra, R. G.; Gati, C.; Laksmono, H.; Dao, E. H.; Gul, S.; Fuller, F.; Kern, J.; Chatterjee, R.; Ibrahim, M.; Brewster, A. S.; et al. Concentric-flow electrokinetic injector enables serial crystallography of ribosome and photosystem II. *Nat Methods* **2016**, *13* (1), 59-62.
16. Lee, D.; Park, S.; Lee, K.; Kim, J.; Park, G.; Nam, K. H.; Baek, S.; Chung, W. K.; Lee, J. L.; Cho, Y.; et al. Application of a high-throughput microcrystal delivery system to serial femtosecond crystallography. *J Appl Crystallogr* **2020**, *53* (Pt 2), 477-485.
17. Liu, Z. Dynamic analysis of center-driven web winder controls. Conference Record of the 1999 IEEE Industry Applications Conference. Thirty-Forth IAS Annual Meeting (Cat. No.99CH36370), Phoenix, AZ, USA, 1999, pp. 1388-1396.
18. Park, J.; Kim, S.; Nam, K. H.; Kim, B.; Ko, I. S. Current status of the CXI beamline at the PAL-XFEL. *J Korean Phys Soc* **2016**, *69* (6), 1089-1093.
19. Kang, H. S.; Min, C. K.; Heo, H.; Kim, C.; Yang, H.; Kim, G.; Nam, I.; Baek, S. Y.; Choi, H. J.; Mun, G.; et al. Hard X-ray free-electron laser with femtosecond-scale timing jitter. *Nat Photonics* **2017**, *11* (11), 708
20. Ko, I. S.; Kang, H. S.; Heo, H.; Kim, C.; Kim, G.; Min, C. K.; Yang, H.; Baek, S. Y.; Choi, H. J.; Mun, G.; et al. Construction and Commissioning of PAL-XFEL Facility. *Appl Sci-Basel* **2017**, *7* (5).

21. Kim, J.; Kim, H. Y.; Park, J.; Kim, S.; Kim, S.; Rah, S.; Lim, J.; Nam, K. H. Focusing X-ray free-electron laser pulses using Kirkpatrick-Baez mirrors at the NCI hutch of the PAL-XFEL. *Journal of Synchrotron Radiation* **2018**, *25*, 289-292.
22. Park, J.; Kim, S.; Kim, S.; Nam, K. H. Multifarious injection chamber for molecular structure study (MICOSS) system: development and application for serial femtosecond crystallography at Pohang Accelerator Laboratory X-ray Free-Electron Laser. *Journal of Synchrotron Radiation* **2018**, *25*, 323-328.
23. White, T. A. Post-refinement method for snapshot serial crystallography. *Philos T R Soc B* **2014**, *369* (1647).
24. White, T. A.; Barty, A.; Liu, W.; Ishchenko, A.; Zhang, H. T.; Gati, C.; Zatsepin, N. A.; Basu, S.; Oberthür, D.; Metz, M.; et al. Serial femto-second crystallography datasets from G protein-coupled receptors. *Sci Data* **2016**, *3*.
25. White, T. A.; Barty, A.; Stellato, F.; Holton, J. M.; Kirian, R. A.; Zatsepin, N. A.; Chapman, H. N. Crystallographic data processing for free-electron laser sources. *Acta Crystallogr D* **2013**, *69*, 1231-1240.
26. White, T. A.; Kirian, R. A.; Martin, A. V.; Aquila, A.; Nass, K.; Barty, A.; Chapman, H. N.: a software suite for snapshot serial crystallography. *Journal of Applied Crystallography* **2012**, *45*, 335-341.
27. Liebschner, D.; Afonine, P. V.; Baker, M. L.; Bunkóczi, G.; Chen, V. B.; Croll, T. I.; Hintze, B.; Hung, L. W.; Jain, S.; McCoy, A. J.; et al. Macromolecular structure determination using X-rays, neutrons and electrons: recent developments in. *Acta Crystallogr D* **2019**, *75*, 861-877.
28. Emsley, P.; Lohkamp, B.; Scott, W. G.; Cowtan, K. Features and development of. *Acta Crystallographica Section D-Biological Crystallography* **2010**, *66*, 486-501.
29. https://www.matweb.com/search/datasheet.aspx?matguid=99c680bc28dd409fb7e8fd3ddbcee537